JACS Au
AN OPEN ACCESS JOURNAL OF THE AMERICAN CHEMICAL SOCIETY

Editors' Choice
Open Access

pubs.acs.org/jacsau
Article

Water Confinement on Polymer Coatings Dictates Proton−Electron Transfer on Metal-Catalyzed Hydrogenation of Nitrite

Pengcheng Huang,△ Yu Yan,△ Ricardo P. Martinho, Leon Lefferts, Bin Wang,* and Jimmy Faria Albanese*

Cite This: JACS Au 2024, 4, 2656−2665
Read Online

ACCESS | Metrics & More | Article Recommendations | Supporting Information

ABSTRACT: Enzymes can precisely control the speed and selectivity of chemical reactions by modifying locally the solvent−reactant interactions. To extrapolate these attributes to heterogeneous catalysts, we have employed thermoresponsive poly *n*-isopropylacrylamide (*p*-NIPAM) brushes bonded to silica spheres containing palladium. These polymers can form hydrogen bonds with water molecules at low temperatures (<32 °C) allowing the polymer to stay swollen. Detailed reaction kinetics of nitrite hydrogenation showed that *p*-NIPAM decreases the apparent activation barrier by a factor of 3 at low temperatures. Diffusion-ordered spectroscopy nuclear magnetic resonance and ab initio molecular dynamics simulations showed that when *p*-NIPAM is present, water molecules near the surface are less mobile. This confinement perturbs the water interaction with the metal, reducing the barrier for the proton−electron transfer reduction of nitrite. Notably, this enhancement vanishes at high temperature as the polymer collapses on itself exposing the Pd to unconfined water. The fully reversible nature of this process opens the door for creating homeostatic catalysts with controlled water-confinement.

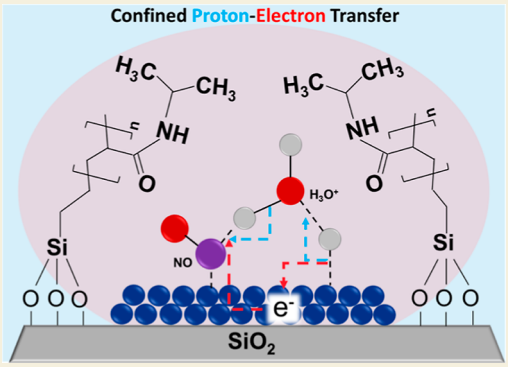

KEYWORDS: *proton−electron transfer, solvation effects, poly(N-isopropylacrylamide), temperature responsive catalysts, homeostatic catalysis, polymer coated catalysts*

INTRODUCTION

Water-catalyst interactions have proven to be critical for catalytic reactions in aqueous environments.[1,2] Enzymes are a prototypical example of fine manipulation of water-active site interaction to achieve high activities and selectivity at mild temperatures. Designing programmable catalysts that can sense the operating environment and manipulate accordingly the activity and selectivity of the active site is a major challenge. Over the past decade, stimulus-responsive polymers that undergo sharp transitions from swollen to collapse state have been used to modify the solubility of a catalyst in the reaction solvent and to change the accessibility of the active site to the reactants. In the first one, the catalyst is recovered by applying an external stimulus (e. g., pH, heat, light, or magnetic fields) that triggers a change in the conformational structure of the polymer from swollen to deswollen, initiating the flocculation and precipitation of the catalyst out of the reaction media. This facilitates the catalyst separation and recycling.[3] In the second approach, the mass transfer of molecules toward the active site is reversibly strained as the polymer collapses onto its globular configuration due to the application of the external stimulus.[4] Removal of the external stimuli leads to the polymer swelling, allowing the unrestricted diffusion of molecules. Because the catalytic activity was regulated by the permeability of the molecules through the polymer, it was possible to convert molecules selectively depending on their solubility in the polymer matrix.[5−7] This enabled an unprecedented level of control over the conversion of molecules based on their interaction with the stimulus-responsive polymer above and below the critical solubility threshold.

The first kinetic model of egg-shell nanoreactors with stimulus-responsive behavior was developed by Carregal-Romero et al.[8] for the electron-transfer reaction between hexacyanoferrate(III) and borohydride ions using Au nanoparticles encapsulated on poly isopropylacrylamide (*p*-NIPAM) with different extents of cross-linking. This polymer has a characteristic lower critical solution temperature limit (LCST) of 32 °C. That means that at temperatures above the LCST the solubility of the polymer in water drastically decreases due to entropic contributions to the Gibbs free energy of the system. In this case, the system was described using a pseudo-first-order kinetic model in which the observed kinetic constant was defined as the result of the coupling of the

Received: May 1, 2024
Revised: May 22, 2024
Accepted: May 22, 2024
Published: June 28, 2024

https://doi.org/10.1021/jacsau.4c00389
JACS Au 2024, 4, 2656−2665

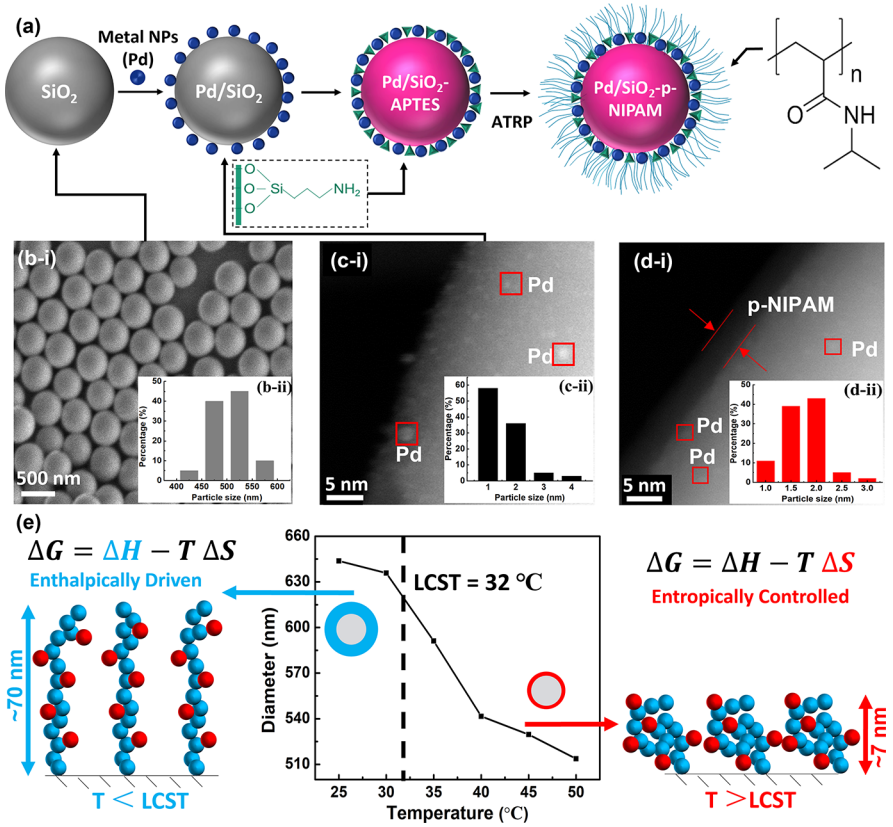

Figure 1. Synthesis strategy for the growth of *p*-NIPAM brushes on Pd/SiO_2 catalysts (a), scanning electron microscopy (SEM) of SiO_2 spheres [b(i)], high-resolution transmission electron microscopy (HR-TEM) of Pd/SiO_2 [c(i)] and Pd/SiO_2-*p*-NIPAM [d(i)] catalysts together with the particle size distribution of SiO_2 [b(ii)] and Pd clusters for uncoated [c(ii)] and polymer-coated catalysts [d(ii)]. Dynamic light scattering (DLS) measurement and schematic diagram of controlled entropy and enthalpy changes at different temperatures (e).

first-order surface reaction kinetics (k_r) and mass transport (k_d) through the polymer layer (eq 1) at temperatures below and above the LCST.

$$k_{obs}^{-1} = k_r^{-1} + k_d^{-1} \quad (1)$$

This work argued that at low temperatures the activation barriers measured were those corresponding to the diffusion of the reactants at infinite dilution in the aqueous media (~10 kJ/mol). At high temperatures (>32 °C), the polymer density increases leading to a drop in the porosity and an increase in tortuosity that lowered the effective diffusion. The authors explained that the observed higher activation barriers were caused by the more difficult diffusion process (~30 kJ/mol). Upon increasing the content of cross-linking in the polymer gel, the extent of gel shrinkage upon reaching the LCST was drastically reduced, which in turn lowered the activation energies previously observed above the LCST. In a subsequent study, the groups of Ballauff and Dzubiella[6] reported that the nature of *p*-NIPAM-reactant interactions exerted a remarkable influence on the rate of reactions, allowing hydrophobic molecules to be converted selectively at high temperatures. This was attributed to a more favorable partition of the hydrophobic reactants into the polymer matrix (i.e., lower Gibbs free energy of transfer from the bulk to the polymer) above the LCST of *p*-NIPAM even under constrained porosity and tortuosity. In this case, the diffusion rate of the limiting reactant through the polymer layer was derived following the Debye−Smoluchowski theory.[7]

The theory predicts that as the *p*-NIPAM environment becomes more hydrophobic above the LCST, the partition of molecules into the polymer matrix increases exponentially for the more hydrophobic reactants, while the opposite occurs for the hydrophilic substrates. This theory has been successfully employed to describe multicomponent reaction processes occurring in stimulus-responsive nanoreactors.[4] The main drawback of this approach is that the interactions between the polymer and surface reacting species are neglected when the system is free of mass transport effects. That is, the kinetics observed in an uncoated catalyst were assumed to be equal to those measured in a polymer-containing catalyst in the solvated state of the polymer (k_r). More recent studies have shown, however, that this simplification leads to important deviations between theory and experimental observations.[9−11] These results indicate that polymer−reactant interactions are key for both diffusion and reaction of molecules when catalysts are functionalized with *p*-NIPAM polymeric brushes.

The present contribution challenges this model and aims at studying the interplay of the polymer-solvation effects on the surface reaction kinetics (k_r) in the absence of any mass transfer limitations (i.e., $k_d \gg k_r$). We developed a Pd-containing catalyst supported on pore-less SiO_2 spheres of ca. 500 nm that contained *p*-NIPAM brushes grown from the surface hydroxyl groups using atom transfer radical polymerization (ATRP). In these catalysts, all Pd atoms are readily available for reaction, and no internal mass transport limitations are expected, as there are no pores. In addition, we employed high mixing rates (500 rpm) to ensure

https://doi.org/10.1021/jacsau.4c00389
JACS Au 2024, 4, 2656−2665

Table 1. Characterization Data of Parent Catalyst (Pd/SiO_2), Polymer-Coated Catalyst (Pd/SiO_2-*p*-NIPAM), and Support Material (SiO_2)

sample	SEM	XRF	CO-chemisorption	TEM		N_2 physisorption	
	particle size (nm)	Pd loading (wt %)	Pd dispersion (%)	mean Pd particle size (nm)	Pd dispersion (%)	specific surface area (m^2/g)	theoretical specific surface area (m^2/g)
SiO_2	500					7.5	6.4
Pd/SiO_2	500	0.17	55.5	2.1	52.0	7.9	6.7
Pd/SiO_2-*p*-NIPAM	500	0.15	19.9	1.9	57.5	9.2	

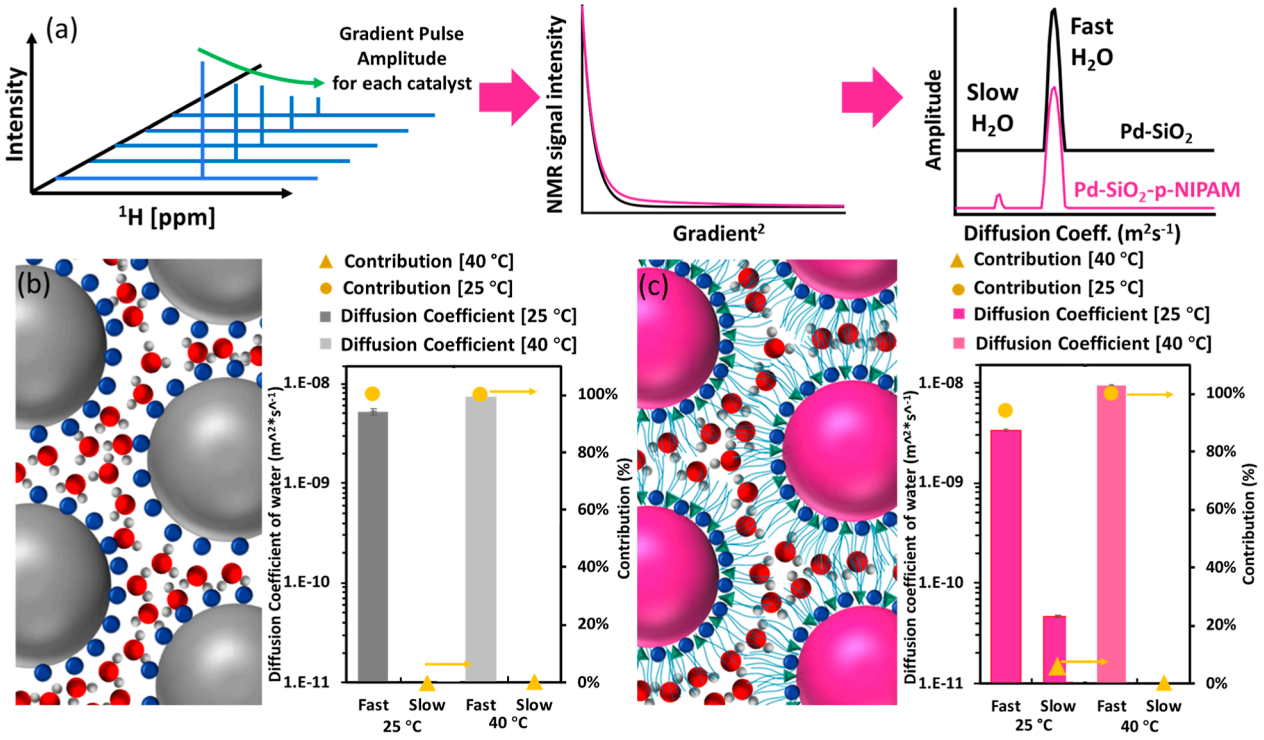

Figure 2. Inverse laplace transform analysis of demonstrative 1H water DOSY NMR data for the particle slurries above and below the LCST. (a) Pictorial representation of the data obtained during a DOSY NMR measurement and subsequent analysis; contribution and diffusion coefficient of the two catalysts at 25 and 40 °C (b) Pd/SiO_2, (c) Pd/SiO_2-*p*-NIPAM, alongside a representative image of their states.

instantaneous equilibration of gaseous reactants in the aqueous slurry of the catalyst, thus eliminating gas−liquid and liquid−solid transport limitations. As proxy of the activity of the metal in the presence of polymers, we studied the hydrogenation of nitrite (NO_2^-) on Pd/SiO_2 with and without *p*-NIPAM brushes. By combining rigorous kinetic measurements, transition state theory treatments, ab initio molecular dynamics (AIMD) simulations, and electrostatics, we have demonstrated that stimulus-responsive polymers can induce solvation effects that alter the apparent reaction barriers for the nitrite hydrogenation by modifying the mobility of water molecules near the active site and the electronic properties near the active sites to different extents depending on the solvation state of the polymer. Here, precise control over the apparent barrier was possible simply by modifying swelling of the *p*-NIPAM brushes with the temperature. These results highlight the important role that water confinement near the active sites has on the reactivity of metal catalysts while opening new opportunities for dynamic manipulation of activity and selectivity using polymer coatings.

RESULTS AND DISCUSSION

Catalyst characterization

The combination of techniques employed to characterize the functionalized Pd catalyst provides a complete picture of their structure and composition. Figure 1a illustrates the growth of *p*-NIPAM brushes on Pd/SiO_2 catalysts by leveraging the surface hydroxyl moieties of the colloidal SiO_2 particles. This structure was confirmed independently using SEM and HR-TEM. From Figure 1b(i), it is clear that SiO_2 particles produced via the Stobër process are nonporous and spherical solids with a narrow particle size distribution of ca. 500 nm. TEM characterization of the parent Pd/SiO_2 and polymer-coated catalyst (Pd/SiO_2-*p*-NIPAM) revealed that the metal clusters were ca. 2 nm (Figure 1c,d).

A slight decrease in the metal cluster size was observed upon functionalization of Pd/SiO_2 with *p*-NIPAM polymers. This drop was attributed to the detachment of larger Pd clusters observed during the polymerization steps. Further TEM-EDS mapping images showed that the Pd particles were well dispersed on the Pd/SiO_2 and Pd/SiO_2-*p*-NIPAM catalysts and that no residues from the ATRP process are left on the surface (Figure S2). The TGA (Figure S1) shows the weight

https://doi.org/10.1021/jacsau.4c00389
JACS Au 2024, 4, 2656−2665

loss increase with polymerization time, and when the polymerization is above 6 h, the polymer length increases slowly. Upon functionalization with the *p*-NIPAM polymeric brushes for over 22 h, it was possible to achieve a polymer dry thickness of ca. 7 nm [Figure 1d(i)]. These observations were in line with DLS measurements, as shown in Figure 1e. The stimulus-responsive behavior of the polymer-coated catalyst (Pd/SiO_2-*p*-NIPAM) was confirmed by measuring the average hydrodynamic diameter of the particles at different temperatures (25 to 50 °C). At temperatures below 30 °C, the particle size remained stable at ca. 640 nm. Increasing the temperature above 32 °C led to a rapid drop in the particle size to ca. 514 nm. This would indicate that the film thickness of the polymer varies from 70 to 7 nm as temperature increases from 25 to 50 °C. In these polymers, the strong interaction of water molecules with the ammine moieties of the polymer dominates at low temperatures (enthalpic driven swelling, Figure 1e left). At high temperatures, the entropic contribution to the Gibbs free energy overtakes the enthalpic affinity, leading to the collapse of the polymer on itself (Figure 1e right).

An interesting characteristic of these pore-less catalysts is that the metal dispersion is essentially unaltered even after the growth of the *p*-NIPAM brushes using ATRP (see Table 1). For the Pd/SiO_2 catalyst, the Pd metal loading was 0.17 wt %, while the Pd dispersion was 56% based on CO chemisorption, corresponding to an average Pd particle size of ca. 2.0 nm. This is in good agreement with the estimated Pd particle size obtained by TEM (ca. 2.1 nm). In the case of Pd/SiO_2-*p*-NIPAM, the mean Pd particle size was similar, ca. 1.9 nm [Figure 1d(ii)]. Surprisingly, the Pd dispersion obtained from CO chemisorption indicated a much lower value (ca. 19.9%). This difference can be associated with the partial blockage of the Pd surface by the polymer brushes during CO chemisorption in the gas phase. Similar observations were reported by Zhao et al.[12] when using poly(vinyl alcohol) (PVA) and polyvinylpyrrolidone to cover Pd nanoparticles during nitrite reduction. To estimate the metal dispersion, we employed the mean particle size obtained from TEM, resulting in a value of 57.5% (Section S6 of the Supporting Information).

Water Mobility in Polymer-Coated Catalysts

Since *p*-NIPAM is a stimulus-responsive polymer that can interact with water molecules in a distinct manner at temperatures above and below the LCST (32 °C), one could use nuclear magnetic resonance (NMR) to determine the mobility of water molecules interacting with the polymer near the surface. To achieve this, the Pd/SiO_2 catalysts with and without *p*-NIPAM coating were dispersed into concentrated slurries with small amounts of water (1.63 g of catalyst/ml). This was equivalent to two water solvation layers on the pore-less catalysts, allowing us to probe the water microenvironment, unlike in previous descriptions.[13] Diffusion-ordered spectroscopy (DOSY) was used to examine the water mobility (Figure 2a). This technique can shed light into the translational motion of molecules, namely, by biexponential fitting of the diffusion decays.[14] This has been successfully used in the past to identify populations of confined water molecules even in small quantities.[15,16]

Diffusional motions of water were investigated herein by inverse Laplace transform to interrogate the multiple environments present in the system. In each experiment, we studied the diffusion of water at low and high temperatures. As it can be observed in Figure 2, for the Pd/SiO_2 catalyst at low and high temperatures, the dominant diffusion coefficient is that of "fast" water, which displayed a diffusivity that similar to that of free water (ca. 2.3×10^{-9} m^2 s^{-1}).[17] In contrast, on the polymer-coated sample, two types of water molecules were observed at low temperatures (Figure 2b,c). At low temperatures (25 °C), a population of "slow" moving water was observed. These water molecules display diffusion coefficients that are 2 orders of magnitude slower than the rest of the water molecules (Table S3). While the fraction of "slow" diffusing water seems small, the drastic change in the diffusion coefficients would indicate that these water molecules are essentially confined inside the *p*-NIPAM layer. Here, one must remember that for these pore-less catalysts ca. 1.2% of the water molecules are influenced by the surface of the particles (Section S10 of Supporting Information). Thus, the observed population of "slow" moving water of 6.4 ± 0.1% is rather significant.

In this scenario, one could argue that this "slow-moving" water does not necessarily interact with the metal supported on the silica but rather with the polymer at the liquid-*p*-NIPAM interface. To rationalize, it is important to consider that the 10-fold swelling observed in our coated catalyst resembles that of silicon-SiO_2 wafers functionalized with *p*-NIPAM at high grafting density.[11,18] That is, on our SiO_2 spheres, one would expect a high number of polymer brushes per unit area. Hence, it is possible that the smaller self-diffusion coefficient of water herein observed is linked to the molecules close to the Pd/SiO_2 surface, where the polymer is highly packed. Notably, at higher temperatures, only "fast" diffusing water molecules could be observed. This would suggest that these local interactions near the interface fade as the polymer collapses on itself.

AIMD Simulations of the Water-Pd-NIPAM Interface

While the altered water mobility in the presence of *p*-NIPAM was experimentally observed using DOSY NMR, the exact molecular arrangement or distribution of the interfacial water at the interface of polymer-coated catalysts remains elusive. We thus performed AIMD simulations to obtain the distribution profile on both catalyst surfaces (i.e., Pd and Pd-*p*-NIPAM). We adopted a very simplified model, in which two NIPAM monomers were included in water to represent the polymer (Figure 3b). The vertical distribution of water with respect to the metal surface is calculated over a 15 ps time window after 25 ps pre-equilibrium (Figure S11). Within the 6 Å range (Figure 3c), there are two peaks observed in both systems, indicating specific water arrangement in the first layer. The first peak located at around 2.3, Å with respect to the surface, corresponding to strong surface-bound water molecules (a). The second peak, water (b) is centered at around 3.0 Å. These water molecules form H-bonds with water detected in the first peak. One of the two NIPAM moieties, located slightly above the first layer of water, was found to narrow the distribution of the interfacial water, which is well represented by the disappearance of the tail in the distribution at around 5 Å (Figure 3c). We further investigated the dynamics of the interfacial water and their interplay with the NIPAM species and reactive intermediate (NO). We first analyzed the vertical movement of water molecules (a) in the presence and absence of *p*-NIPAM to compare the mobility of water molecules (Figures 3d and S13).

https://doi.org/10.1021/jacsau.4c00389
JACS Au 2024, 4, 2656−2665

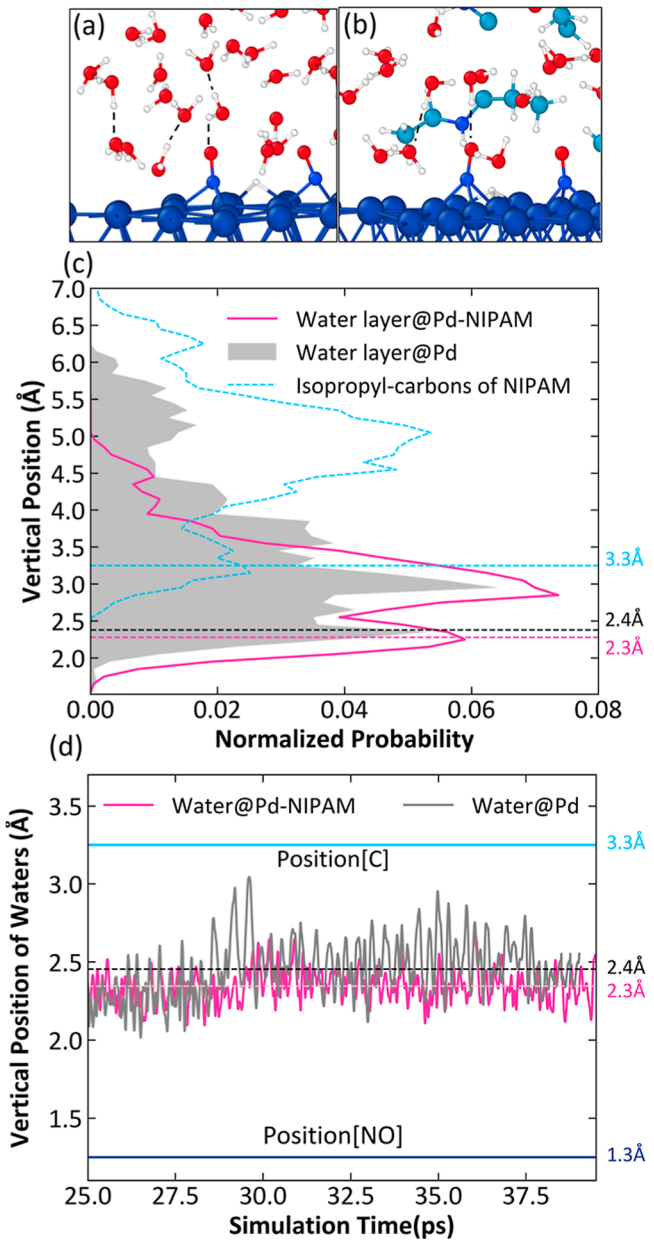

Figure 3. (a,b) Atomic structure of the water interface on Pd and Pd-*p*-NIPAM with surface-adsorbed NO, a key reaction intermediate. Element colors (Pd: deep blue; C: cyan; H: white; O: red; and N: blue). (c) The interfacial water layer distribution above the metal surface at the Pd-water interface (shaded area) and Pd-NIPAM-water interface (solid lines). The intergrate area under each line (area) equal to one. The first peak indicates the interfacial water layer. (d) Dynamic interactions of interfacial H_2O molecules. The dash line presents the position of water layer average to time. The solid line presents the location of one NIPAM monomer presented by the carbon and the reactant intermediate NO presented by the O averaged over AIMD simulations.

Here, we obtained a slightly reduced motion along the vertical direction for the surface "bound" water molecules (a) in the presence of NIPAM moieties. While it is true that the vertical diffusion obtained in AIMD cannot be directly compared with the NMR data, the results herein are consistent with the reduced mobility of water in the presence of the polymer.

The relative difference in the calculated mean square displacement (MSD) of interfacial water as shown in Figure S13 is very subtle as compared to the diffusivity measurement in DOSY, which is likely due to the fact that we only had two NIPAM moieties rather than the real NIPAM polymer in the AIMD simulations. Furthermore, considerable differences are observed when the vertical dynamics of individual water molecules are analyzed with average value. As shown in Figure 3d, for the waters (a) contributing to the first peak at 2.3 Å, the presence of NIPAM (located at 3.3 Å) appears to restrict their vertical diffusion away from the surface. That is, the dynamic distribution of surface-bound water has been confined by the carbon chain in the NIPAM to a narrower distribution than it is otherwise in the absence of NIPAM. Our analysis on the MSD suggests that the presence of NIPAM introduces slow dynamics of the water molecules directly in contact with the metal, which is qualitatively in line with the experimentally observed smaller diffusivity at the Pd-water-NIPAM interface at the low temperatures (Figure S13).

Effect of *p*-NIPAM on Reaction Kinetic

Considering the change in water mobility and its interaction with the metal surface on the *p*-NIPAM coated catalyst, one expects this catalyst to perform differently when changing the temperature is changed above and below the LCST. To study this effect, we conducted a detailed kinetic study on the reactant concentration and temperature using Pd/SiO_2 and Pd/SiO_2-*p*-NIPAM catalysts over a broad range of hydrogen pressures and nitrite concentration.

Before we dive into kinetic data, keep in mind that internal and external mass transfer effects have been excluded under the reaction conditions herein employed, allowing us to confine our findings to the kinetic regime (Section S7 of the Supporting Information). First, we studied the impact of the polymer on the selectivity of the reaction. Here, it was observed that, at the same conversion level (ca. 10%), increasing the temperature led to higher ammonium selectivity on both catalysts. This trend agrees with previous literature on reduction of nitrites using Pd catalyst.[19,20] Notably, in the presence of polymer a significant enhancement in ammonia selectivity was observed (ca. 4-fold higher) regardless of the temperature employed (Figure S4). This suggests that the *p*-NIPAM polymer brushes promote NH_4^+ formation. In this reaction, the ratio of nitrogen to ammonia selectivity is determined by the hydrogen and NO surface coverage. Essentially, when higher hydrogen coverages or lower NO coverage are present NH_4^+ formation increases at the expense of nitrogen.[21−23]

To decode the underlying cause for these differences in selectivity, we employed rigorous reaction order investigations on the Pd/SiO_2 and Pd/SiO_2-*p*-NIPAM catalysts (Figure 4). For this purpose, we employed two temperatures (25 and 50 °C) and in the case of NO_2^-, we assessed the effect of the partial pressure of hydrogen by measuring the reaction orders between 0.03 and 0.8 bar.

The reaction order of nitrite on Pd/SiO_2 at a high hydrogen partial pressure (0.8 bar) varied from 0.7 to 0 as the concentration of nitrite increased. This trend was observed at low (25 °C) and high (50 °C) temperatures. For the Pd/SiO_2-*p*-NIPAM catalyst, a different trend was observed when varying the temperature. At temperatures below the LCST (25 °C), first-order kinetics in nitrite was observed. In this case, increasing the nitrite concentration further led to saturation

https://doi.org/10.1021/jacsau.4c00389
JACS Au 2024, 4, 2656−2665

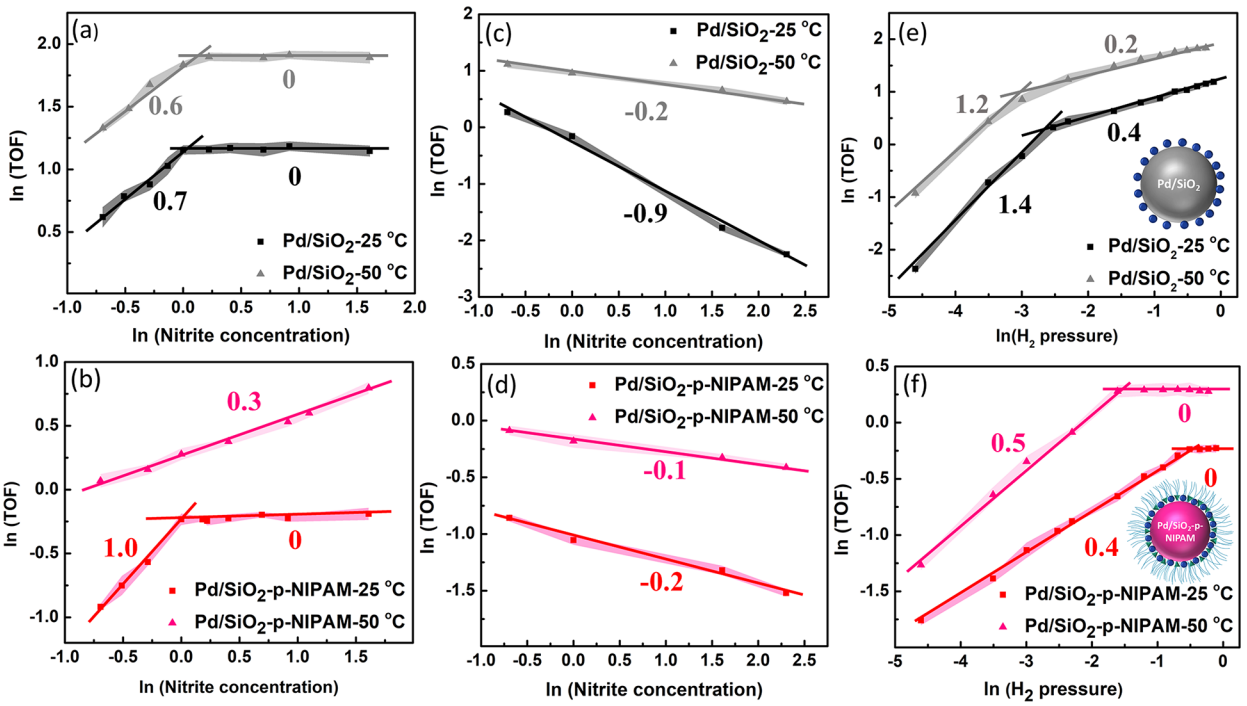

Figure 4. Effect of nitrite concentration on the TOF using Pd/SiO_2 and Pd/SiO_2-*p*-NIPAM catalysts with 0.8 bar H_2 (a,b) and 0.03 bar H_2 (c,d); effect of hydrogen pressure on the TOF at 1 mM nitrite concentration (e,f).

kinetics as indicated by the plateau of the TOF. Notably, at temperatures above the LCST, when the polymer becomes hydrophobic and collapses, there was no inflection point, and the reaction order was ca. 0.3 across the concentration window herein explored. Negative reaction orders in nitrite were observed on both catalysts when the reaction was conducted at a lower hydrogen partial pressure (Figure 4c,d). The negative reaction orders suggest that hydrogen and nitrite compete for the same active sites on both catalysts. Detailed inspection of the data reveals that in the Pd/SiO_2-*p*-NIPAM catalyst, nearly zero-order dependence with nitrite concentration was observed with values of −0.2 and −0.1 at 25 and 50 °C, respectively. These less−negative reaction orders in the *p*-NIPAM coated catalysts can be attributed to weaker interaction of nitrite or nitrite-derived surface species on palladium.

For the hydrogen order investigation, initially a positive reaction order of ca. 1.4 and 1.2 was observed at low and high temperatures, respectively (Figure 4e). When the hydrogen pressure ranged from 0.01 to 0.1 bar on Pd/SiO_2. Increasing further the hydrogen partial pressure decreased the order to ca. 0.5. These high hydrogen orders on Pd/SiO_2 at low pressures are key, as explained in our previously work[24] suggests that there are two colimiting steps determining the rate of the nitrite hydrogenation, including the sequential hydrogen insertion on NO* as well as HNO* surface species. The detailed derivations are shown in the Section S8 of the Supporting Information. In sharp contrast, in the case of polymer-coated catalysts, the reaction rate showed a weaker dependence on the hydrogen pressure. In fact, at hydrogen pressures above 0.5 bar, the reaction order dropped from ca. 0.5 to 0 at 25 °C. These data indicate that increasing the temperature above the LCST of *p*-NIPAM to 50 °C leads to an early onset of saturation kinetics, which suggests higher surface coverages of hydrogen (Table S1). These results would support the idea that in the presence of *p*-NIPAM the higher selectivity toward ammonium is induced by the larger concentration of hydrogen and/or lower NO coverage on the catalyst surface.

Effect of *p*-NIPAM on the Apparent Energy Barriers

To connect the observations on water mobility and selectivity to the presence of polymer coatings, we estimated the apparent barriers at temperatures below and above the LCST of the *p*-NIPAM using low and high concentrations of hydrogen in the range of 22 to 50 °C. As expected, for the Pd/SiO_2 catalyst a constant activation energy barrier was observed throughout the entire temperature range (Figure 5). When the reaction was

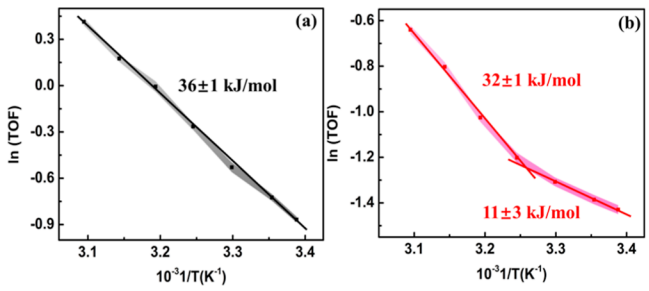

Figure 5. Arrhenius plots for the nitrite hydrogenation using (a) Pd/SiO_2 and (b) Pd/SiO_2-*p*-NIPAM at 0.03 bar hydrogen pressure and 1 mM nitrite concentration.

conducted at low hydrogen pressure (0.03 bar), the apparent energy barrier was 36 ± 1 kJ mol^{-1}. This value is slightly higher than those reported in the literature (23, 26, and 31 kJ mol^{-1}).[19,20,25] Here, one should consider that this energy barrier was obtained at low hydrogen pressure, while the values in the literature were obtained at a higher hydrogen partial pressure (e.g., 0.32 bar). In fact, we observed that when the reaction was conducted at 0.6 bar (Figure S3a), the activation energy barrier decreased to 29 ± 1 kJ mol^{-1}, highlighting the

https://doi.org/10.1021/jacsau.4c00389
JACS Au 2024, 4, 2656−2665

Table 2. Enthalpy and Entropy of Activation for the Pd/SiO_2 and Pd/SiO_2-*p*-NIPAM Catalysts and Excess Enthalpy and Entropy Estimated for the Polymer-Coated Catalyst

temperature (°C)	Pd/SiO_2		Pd/SiO_2-*p*-NIPAM		excess	
	$\Delta S_{App}^{0,\ddagger}$ (J/mol K^{-1})	$\Delta H_{App}^{0,\ddagger}$ (kJ/mol)	$\Delta S_{App}^{p\text{-NIPAM},\ddagger}$ (J/mol K^{-1})	$\Delta H_{App}^{p\text{-NIPAM},\ddagger}$ (kJ/mol)	$\Delta S_{App}^{0,\ddagger}$ (J/mol K^{-1})	$\Delta H_{App}^{0,\ddagger}$ (kJ/mol)
22−32	−34.8	36.4	−124.2	11.4	−89.4	−25.0
32−50			−58.4	31.6	−23.6	−4.8

importance of surface coverage on the apparent barriers for this reaction.

Strikingly, the polymer-coated catalyst showed two distinct activation energies as the temperature increased (Figure 5b). Essentially, when the reaction was conducted at temperatures below the LCST of *p*-NIPAM (swollen state), a low apparent activation barrier of 11 kJ mol^{-1} was observed. Increasing the temperature above the LCST (collapse state) led to a higher apparent barrier (about 32 kJ mol^{-1}). The lower activation energy barriers obtained when the polymer was in the swollen state suggests that there is a strong link between water confinement and the catalytic activity of metal-supported catalysts.

Estimation of Polymer-Induced Solvation Effects

To assess the nonidealities of the solvation layer near the active sites one could use transition state theory treatments as proposed by Flaherty et al.[26] In this case, we leverage the kinetic observations and the detailed reaction kinetics to derive the rate expression (2). The detailed derivation is shown in Section S9 of the Supporting Information.

$$\frac{r}{L} = \frac{k_b T}{h}\exp\left(\frac{\Delta S_{App}^{0,\ddagger} + \Delta S_{App}^{\varepsilon,\ddagger}}{R}\right)\exp\left(-\frac{\Delta H_{App}^{0,\ddagger} + \Delta H_{App}^{\varepsilon,\ddagger}}{RT}\right)[H_2]^{3/2}[NO_2^-]^{-1} \quad (2)$$

Here, L is the total number of active sites, r/L = TOF, k_b is the Boltzmann constant, h is the Planck constant, T is thermodynamic temperature, and $\Delta S_{App}^{0,\ddagger}$ and $\Delta H_{App}^{0,\ddagger}$ are the enthalpy and entropy of the transition state in the reference state. Here, the initial state is that of the reactants in the liquid phase, while the end state corresponds to the activated complex. The estimated excess entropy ($\Delta S_{App}^{0,\ddagger}$) and enthalpy ($\Delta H_{App}^{\varepsilon,\ddagger}$) of activation in the polymer coated catalyst is obtained by assuming that the parent catalyst (Pd/SiO_2) is the reference state. Here, one can estimate the excess quantities using the results obtained for the polymer-coated catalyst (Figure S10a). The implicit assumption in this equation is that the polymer coating on the Pd/SiO_2-*p*-NIPAM catalyst is responsible for the observed $\Delta S_{App}^{0,\ddagger}$ and $\Delta H_{App}^{0,\ddagger}$ for the reaction (Table 2).

This analysis reveals that when the reaction is conducted at low temperatures (22−32 °C), below the LCST of *p*-NIPAM, there is an enthalpic enhancement of the reaction rate. Essentially, the enthalpy of activation for the transition state decreased by ca. 25 kJ mol^{-1} on the Pd/SiO_2-*p*-NIPAM.

This stabilization, however, comes at the expense of losing degrees of freedom in the system, which causes a drop in the entropy of activation. Here, one could imagine that when the polymer is present, the arrangement and mobility of the water molecules surrounding the chemisorbed species are modified. As a result, the rate toward hydrogenation of the species is altered as well. In our previous study,[24] we showed that water plays a key role in this reaction by facilitating the hydrogenation via proton−electron transfer (PET). To explore the interplay of the reaction kinetics with the nature of the water, the reaction was conducted using D_2O and D_2 to replace H_2O and H_2 (see Section S11 of the Supporting Information).

The results show a strong kinetic isotope effect (KIE) for the Pd/SiO_2-*p*-NIPAM catalyst at 25 and 50 °C with values of 2.1 and 2.6, respectively, while in the case of the uncoated catalyst these values were 2.4 and 1.5 for the same temperatures (Table S4). While the differences between the two catalysts at low temperatures are minor, the strong KIE indicates that hydrogen is involved in the rate-determining step (RDS). Here, one would argue that either hydrogen from the gas or the liquid water could be involved in the RDS. Recently, we reported that these KIE effects and temperature-dependent barriers are also observed during the reduction of nitrobenzene in water, ethanol, and water-NMP solutions when using Pd/SiO_2-*p*-NIPAM.[10] When proton donating solvents were employed, the reaction rates were substantially higher than those observed on the nonprotonic solvents. Furthermore, when using D_2O and D_2 gas, a rather strong KIE is observed on coated and uncoated catalyst, while in the case of H_2O and D_2 gas, the effect was negligible, suggesting the water is involved in the RDS. Similar observations have been made by others when studying hydrogenation reactions of metals supported on zeolites. In these studies, when water and deuterium gas were employed, the KIE diminished, which is in line with the herein proposed proton−electron transfer mechanism.

At this point, however, we still miss the fundamental link between *p*-NIPAM and the surface chemisorbed species (NO* and H*), which ultimately define the barriers for the reaction. For this reason, we examined the surface species binding on the Pd surface for both Pd/SiO_2 and Pd/SiO_2-*p*-NIPAM using AIMD simulations (Figure 6c). The strength of surface binding is manifested by the vibration frequency of surface H in vacuum, water, and water with *p*-NIPAM. Through Fourier Transform analysis of the vertical height of surface-bound hydrogen relative to the Pd surface in vacuum, we obtained a vertical frequency of hydrogen vibration of ca. 30 THz Figure S14. This result agrees with previously measured perpendicular vibrational mode of hydrogen bonded in a 3-fold hollow site over clean Pd surfaces.[27] Next, we studied how the presence of *p*-NIPAM affected the vertical motion of hydrogen at the Pd-water interface. The competitive adsorption of water and hydrogen has been discussed in literature as the interfacial charge transfer between water and metal may destabilize the surface hydrogen adsorption.[28] The extent of destabilization can be interpreted in terms of Stark effects in which the local electric field induced by the presence of the water is strongly coupled to molecular orientation at the interface.[29]

Notably, upon addition of *p*-NIPAM, the hydrogen vertical vibrational frequency shifts to slightly lower values, and the

https://doi.org/10.1021/jacsau.4c00389
JACS Au 2024, 4, 2656−2665

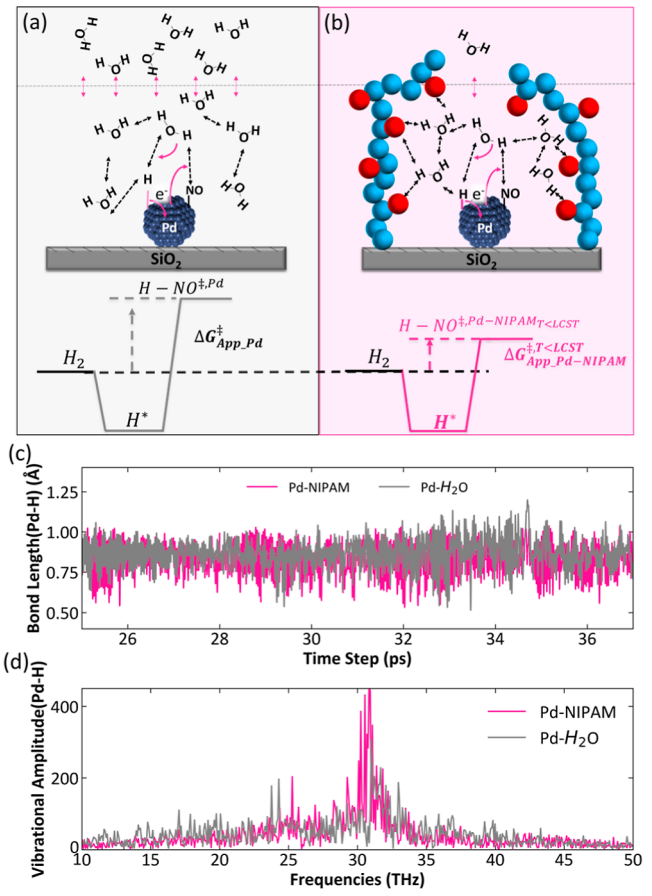

Figure 6. Illustration of the water−catalyst interactions near the metal active sites and the corresponding change in hydrogen activation for (a) Pd/SiO_2 and (b) Pd/SiO_2-*p*-NIPAM (not at scale). (c) AIMD simulations of the vertical height of surface-adsorbed hydrogen, defined by the vertical distance between hydrogen and the Pd(111) surface in Pd/SiO_2 (gray) and Pd/SiO_2-*p*-NIPAM (pink). (d) The vertical vibrational frequency analysis of the H on Pd.

peak becomes sharper (Figure 6d). This suggests that the more structured water in the presence of *p*-NIPAM facilitates the interaction between the interfacial water and surface hydrogen. This is a rather unexpected result as one would anticipate that for the polymer to induce a reduction in the apparent barrier, the bonding of the species prior the transition state must be stronger. In fact, previous work has shown drastic changes in the apparent barriers as pH was varied from acidic to basic,[30] which was attributed to the reorganization of water molecules and the alteration of local electric fields.[31] Here, one must keep in mind that these observations were reported when changing the concentration of protons by several orders of magnitude (2−3 to 10−12), which is not the case in the present study. We intentionally controlled the pH by continuously feeding carbon dioxide as a buffer.

Alternatively, one could imagine that *p*-NIPAM binds to metal and modifies the binding of the kinetically relevant species, as reported in the case of self-assembled monolayers. This type of ligand effect is often reported in the case of sulfide-containing molecules that strongly bind to the metal, altering the site accessibility and surface binding. However, in previous studies, we showed via XPS characterization that *p*-NIPAM does not change the electronic structure of Pd.[9−11] Hence, these differences emerge only when water molecules are present, suggesting that the ligand effect cannot explain these results.

In this line, the subtle effect of *p*-NIPAM on the hydrogen binding would suggest that changes in the apparent barriers and reaction orders are linked with both the energetics of the transition state and the binding of the reactive species.

To rationalize this proposition, one must note that the surface hydrogen is shuttled to the NO through the H-bonded water network via a positively charged transition state. This more pronounced interaction between H and the confined water can thus assist the proton shuttling. The positively charged transition state is further stabilized by a larger dielectric constant in the presence of *p*-NIPAM (see discussion in Section S16 and Figure S15). This combined effect likely reduced the true barrier required to form the activated complex (Figure 6a,b). Meanwhile, the tighter interaction between the transition state and this more structured water likely leads to reduced entropy of the transition state, in line with the observed lower entropy of activation (see Table 2), following an enthalpy−entropy compensation. While it is true that at this stage our argumentation is speculative, we hope that it can trigger further discussions on the underlying effects that water confinement can induce on catalytic systems containing polymeric coatings.

CONCLUSIONS

We have demonstrated that water confined in polymeric films can induce reversible changes in the microsolvation environment near the surface metal catalysts. When these coatings are based on thermoresponsive polymers (e. g., *p*-NIPAM) the behavior can be tuned simply by changing the operating temperature. DOSY NMR characterization indicated that the population of slowly diffusing water molecules is significant when the polymer is swollen at low temperatures. The lower mobility of water was confirmed by AIMD calculations that showed that on these catalysts, water molecules are essentially confined by the polymer near the metal surface. The confined water is strongly interacting with *p*-NIPAM polymers, which decreases the strong electric fields induced by the presence of water molecules near the metal surface. This favors the stabilization of the transition state, lowering the apparent barriers of activation while increasing the ammonium selectivity when the polymer is in the swollen state. Upon collapsing at temperatures above the LCST the polymer−water interactions are disrupted, and the structure of the water molecules near the active sites returns to its original configuration, leading to higher barriers and lower ammonium selectivity. We anticipate that these results will pave the way for developing programmable catalysts capable of mimicking the self-regulating nature, high activity, and quantitative selectivity of enzymes.

ASSOCIATED CONTENT

Supporting Information

The Supporting Information is available free of charge at https://pubs.acs.org/doi/10.1021/jacsau.4c00389.

Full details of the catalyst characterization, materials and methods, catalyst preparation, mass transfer assessment, kinetic measurements, NMR analysis, and AIMD simulations (PDF)

https://doi.org/10.1021/jacsau.4c00389
JACS Au 2024, 4, 2656−2665

AUTHOR INFORMATION

Corresponding Authors

Bin Wang − *School of Chemical, Biological and Materials Engineering, University of Oklahoma, Norman, Oklahoma 73019, United States;* orcid.org/0000-0001-8246-1422; Email: wang_cbme@ou.edu

Jimmy Faria Albanese − *Catalytic Processes and Materials Group, Faculty of Science and Technology, MESA+ Institute for Nanotechnology, University of Twente, Enschede 7500 AE, The Netherlands;* orcid.org/0000-0002-8920-3538; Email: j.a.fariaalbanese@utwente.nl

Authors

Pengcheng Huang − *Jiangsu Key Laboratory of Advanced Catalytic Materials and Technology, School of Petrochemical Engineering, Changzhou University, Changzhou 213164, PR China;* orcid.org/0000-0003-2211-2217

Yu Yan − *School of Chemical, Biological and Materials Engineering, University of Oklahoma, Norman, Oklahoma 73019, United States*

Ricardo P. Martinho − *Department of Molecules and Materials, MESA+ Institute for Nanotechnology, Faculty of Science and Technology, University of Twente, Enschede 7500 AE, The Netherlands;* orcid.org/0000-0003-4223-174X

Leon Lefferts − *Catalytic Processes and Materials Group, Faculty of Science and Technology, MESA+ Institute for Nanotechnology, University of Twente, Enschede 7500 AE, The Netherlands;* orcid.org/0000-0003-2377-5282

Complete contact information is available at: https://pubs.acs.org/10.1021/jacsau.4c00389

Author Contributions

△P.H. and Y.Y. contributed equally to this paper. The manuscript was written through contributions of all authors. All authors have given approval to the final version of the manuscript.

Notes

The authors declare no competing financial interest.

ACKNOWLEDGMENTS

The authors gratefully acknowledge the financial support from Jiangsu Key Laboratory of Advanced Catalytic Materials and Technology (BM2012110). We are grateful to Rodrigo Fernández-Pacheco from Zaragoza University for the TEM analysis, K. Altena−Schildkamp for chemical analysis. B. Geerdink for technical support. The simulation was performed at the OU Supercomputing Center for Education & Research and the National Energy Research Scientific Computing Center (NERSC), a U.S. Department of Energy Office of Science User Facility. The work was also supported by the U.S. Department of Energy, Basic Energy Sciences, Catalysis Science (grant DE-SC0018284).

REFERENCES

(1) Li, G.; Wang, B.; Resasco, D. E. Solvent Effects on Catalytic Reactions and Related Phenomena at Liquid-Solid Interfaces. *Surf. Sci. Rep.* **2021**, *76* (4), 100541.

(2) Li, G.; Wang, B.; Resasco, D. E. Water-Mediated Heterogeneously Catalyzed Reactions. *ACS Catal.* **2020**, *10* (2), 1294−1309.

(3) Zhang, J.; Zhang, M.; Tang, K.; Verpoort, F.; Sun, T. Polymer-Based Stimuli-Responsive Recyclable Catalytic Systems for Organic Synthesis. *Small* **2014**, *10* (1), 32−46.

(4) Hervés, P.; Pérez-Lorenzo, M.; Liz-Marzán, L. M.; Dzubiella, J.; Lu, Y.; Ballauff, M. Catalysis by Metallic Nanoparticles in Aqueous Solution: Model Reactions. *Chem. Soc. Rev.* **2012**, *41* (17), 5577.

(5) Roa, R.; Kim, W. K.; Kanduč, M.; Dzubiella, J.; Angioletti-Uberti, S. Catalyzed Bimolecular Reactions in Responsive Nanoreactors. *ACS Catal.* **2017**, *7* (9), 5604−5611.

(6) Wu, S.; Dzubiella, J.; Kaiser, J.; Drechsler, M.; Guo, X.; Ballauff, M.; Lu, Y. Thermosensitive Au-PNIPA Yolk-Shell Nanoparticles with Tunable Selectivity for Catalysis. *Angew. Chem., Int. Ed.* **2012**, *51* (9), 2229−2233.

(7) Angioletti-Uberti, S.; Lu, Y.; Ballauff, M.; Dzubiella, J. Theory of Solvation-Controlled Reactions in Stimuli-Responsive Nanoreactors. *J. Phys. Chem. C* **2015**, *119* (27), 15723−15730.

(8) Carregal-Romero, S.; Buurma, N. J.; Pérez-Juste, J.; Liz-Marzán, L. M.; Hervés, P. Catalysis by Au@pNIPAM Nanocomposites: Effect of the Cross-Linking Density. *Chem. Mater.* **2010**, *22* (10), 3051−3059.

(9) da Silva, M. J. E.; Lefferts, L.; Faria Albanese, J. A. N-Isopropylacrylamide Polymer Brushes Alter the Micro-Solvation Environment during Aqueous Nitrite Hydrogenation on Pd/Al2O3 Catalyst. *J. Catal.* **2021**, *402*, 114−124.

(10) Huang, P.; Betting, J.; Tian, S.; Lefferts, L.; Faria Albanese, J. Modifying Reaction Rates and Stimulus-Responsive Behavior of Polymer-Coated Catalysts Using Aprotic Solvents. *J. Catal.* **2023**, *428*, 115157.

(11) Enes da Silva, M. J.; Banerjee, A.; Lefferts, L.; Faria Albanese, J. A. In-Situ ATR-IR Spectroscopy Reveals Complex Absorption-Diffusion Dynamics in Model Polymer-Membrane-Catalyst Assemblies (PCMA). *ChemCatChem* **2022**, *14* (10), No. e202101835.

(12) Zhao, Y.; Baeza, J. A.; Koteswara Rao, N.; Calvo, L.; Gilarranz, M. A.; Li, Y. D.; Lefferts, L. Unsupported PVA-and PVP-Stabilized Pd Nanoparticles as Catalyst for Nitrite Hydrogenation in Aqueous Phase. *J. Catal.* **2014**, *318*, 162−169.

(13) Huang, P.; Baldenhofer, R.; Martinho, R. P.; Lefferts, L.; Faria Albanese, J. A. Stimulus-Responsive Control of Transition States on Nanohybrid Polymer-Metal Catalysts. *ACS Catal.* **2023**, *13*, 6590−6602.

(14) Brand, T.; Cabrita, E.; Berger, S. Intermolecular interaction as investigated by NOE and diffusion studies. *Prog. Nucl. Magn. Reson. Spectrosc.* **2005**, *46*, 159−196.

(15) Nelson, M. L.; Romo, J. E.; Wettstein, S. G.; Seymour, J. D. Impact of Xylose on Dynamics of Water Diffusion in Mesoporous Zeolites Measured by NMR. *Molecules* **2021**, *26* (18), 5518.

(16) Beckert, S.; Stallmach, F.; Toufar, H.; Freude, D.; Kärger, J.; Haase, J. Tracing Water and Cation Diffusion in Hydrated Zeolites of Type Li-LSX by Pulsed Field Gradient NMR. *J. Phys. Chem. C* **2013**, *117* (47), 24866−24872.

(17) Holz, M.; Heil, S. R.; Sacco, A. Temperature-dependent self-diffusion coefficients of water and six selected molecular liquids for calibration in accurate 1H NMR PFG measurements. *Phys. Chem. Chem. Phys.* **2000**, *2*, 4740−4742.

(18) Yu, Y.; Kieviet, B. D.; Liu, F.; Siretanu, I.; Kutnyánszky, E.; Vancso, G. J.; De Beer, S. Stretching of Collapsed Polymers Causes an Enhanced Dissipative Response of PNIPAM Brushes near Their LCST. *Soft Matter* **2015**, *11* (43), 8508−8516.

(19) Höller, V.; Rådevik, K.; Yuranov, I.; Kiwi-Minsker, L.; Renken, A. Reduction of Nitrite-Ions in Water over Pd-Supported on Structured Fibrous Materials. *Appl. Catal., B* **2001**, *32* (3), 143−150.

(20) Pintar, A.; Berčič, G.; Levec, J. Catalytic Liquid-phase Nitrite Reduction: Kinetics and Catalyst Deactivation. *AIChE journal* **1998**, *44* (10), 2280−2292.

(21) Postma, R. S.; Brunet Espinosa, R.; Lefferts, L. Competitive Adsorption of Nitrite and Hydrogen on Palladium during Nitrite Hydrogenation. *ChemCatChem* **2018**, *10*, 3770−3776.

(22) Zhao, Y.; Koteswara Rao, N.; Lefferts, L. Adsorbed Species on Pd Catalyst during Nitrite Hydrogenation Approaching Complete Conversion. *J. Catal.* **2016**, *337*, 102−110.

(23) Ebbesen, S. D.; Mojet, B. L.; Lefferts, L. In Situ ATR-IR Study of Nitrite Hydrogenation over Pd/Al2O3. *J. Catal.* **2008**, *256* (1), 15−23.
(24) Huang, P.; Yan, Y.; Banerjee, A.; Lefferts, L.; Wang, B.; Faria Albanese, J. A. Proton Shuttling Flattens the Energy Landscape of Nitrite Catalytic Reduction. *J. Catal.* **2022**, *413*, 252−263.
(25) Chinthaginjala, J. K.; Lefferts, L. Support Effect on Selectivity of Nitrite Reduction in Water. *Appl. Catal., B* **2010**, *101* (1−2), 144−149.
(26) Potts, D. S.; Bregante, D. T.; Adams, J. S.; Torres, C.; Flaherty, D. W. Influence of Solvent Structure and Hydrogen Bonding on Catalysis at Solid-Liquid Interfaces. *Chem. Soc. Rev.* **2021**, *50* (22), 12308−12337.
(27) Conrad, H.; Kordesch, M. E.; Scala, R.; Stenzel, W. Surface Resonances on Pd(111)/H Observed with HREELS. *Stud. Surf. Sci. Catal.* **1986**, *26* (C), 289−298.
(28) Surendralal, S.; Todorova, M.; Neugebauer, J. Impact of Water Coadsorption on the Electrode Potential of H-Pt(1 1 1)-Liquid Water Interfaces. *Phys. Rev. Lett.* **2021**, *126* (16), 166802.
(29) Head-Gordon, M.; Tully, J. C. Electric Field Effects on Chemisorption and Vibrational Relaxation of CO on Cu(100). *Chem. Phys.* **1993**, *175* (1), 37−51.
(30) Singh, N.; Lee, M. S.; Akhade, S. A.; Cheng, G.; Camaioni, D. M.; Gutiérrez, O. Y.; Glezakou, V. A.; Rousseau, R.; Lercher, J. A.; Campbell, C. T. Impact of PH on Aqueous-Phase Phenol Hydrogenation Catalyzed by Carbon-Supported Pt and Rh. *ACS Catal.* **2019**, *9* (2), 1120−1128.
(31) Wesley, T. S.; Román-Leshkov, Y.; Surendranath, Y. Spontaneous Electric Fields Play a Key Role in Thermochemical Catalysis at Metal-Liquid Interfaces. *ACS Cent. Sci.* **2021**, *7* (6), 1045−1055.

https://doi.org/10.1021/jacsau.4c00389
JACS Au 2024, 4, 2656−2665